© 2016. Published by The Company of Biologists Ltd | Journal of Cell Science (2016) 129, 1305-1311 doi:10.1242/jcs.180885

SHORT REPORT

HDAC6 regulates the dynamics of lytic granules in cytotoxic T lymphocytes

Norman Núñez-Andrade[1,2], Salvador Iborra[3], Antonio Trullo[4,5], Olga Moreno-Gonzalo[1,2], Enrique Calvo[6], Elena Catalán[7], Gaël Menasche[8], David Sancho[3], Jesús Vázquez[6], Tso-Pang Yao[9], Noa Beatriz Martín-Cófreces[1,2,*] and Francisco Sánchez-Madrid[1,2,*,‡]

ABSTRACT

HDAC6 is a tubulin deacetylase involved in many cellular functions related to cytoskeleton dynamics, including cell migration and autophagy. In addition, HDAC6 affects antigen-dependent CD4$^+$ T cell activation. In this study, we show that HDAC6 contributes to the cytotoxic function of CD8$^+$ T cells. Immunization studies revealed defective cytotoxic activity *in vivo* in the absence of HDAC6. Adoptive transfer of wild-type or *Hdac6*$^{-/-}$ CD8$^+$ T cells to *Rag1*$^{-/-}$ mice demonstrated specific impairment in CD8$^+$ T cell responses against vaccinia infection. Mechanistically, HDAC6-deficient cytotoxic T lymphocytes (CTLs) showed defective *in vitro* cytolytic activity related to altered dynamics of lytic granules, inhibited kinesin-1–dynactin-mediated terminal transport of lytic granules to the immune synapse and deficient exocytosis, but not to target cell recognition, T cell receptor (TCR) activation or interferon (IFN)γ production. Our results establish HDAC6 as an effector of the immune cytotoxic response that acts by affecting the dynamics, transport and secretion of lytic granules by CTLs.

KEY WORDS: Histone deacetylase 6, Kinesin 1, Lytic granule

INTRODUCTION

Cytotoxic T lymphocytes (CTLs) are a specialized population of CD8$^+$ T cells that provides defense against virus-infected cells and tumors. Naïve CD8$^+$ T cells differentiate into CTLs upon antigen recognition, a process involving the synthesis and storage of cytotoxic mediators into lysosomal-derived lytic granules (Williams and Bevan, 2007). CTLs eliminate target cells by different mechanisms, including secretion of pro-inflammatory cytokines [e.g. tumor necrosis factor (TNFα) or interferon (IFN)γ; de Saint Basile et al., 2010] and FAS-L (FAS ligand; officially known as FASLG) ligation to its receptor, as well as granule-mediated apoptosis upon cell–cell contact and immune synapse formation (Ritter et al., 2013). Lytic granules fuse with the plasma membrane and release granzymes, cathepsins and perforins (Prf proteins) (Lopez et al., 2013; Pardo et al., 2009). The immune synapse acts as a focal point for exocytosis of lytic granules. Lytic granule polarization towards the target cell depends on T cell receptor (TCR) engagement, driven by the relocation of the centrosome to immune synapse. The lytic granules degranulate at a secretory domain adjacent to the TCR-enriched region within the immune synapse (de Saint Basile et al., 2010; Ritter et al., 2013).

Histone deacetylase 6 (HDAC6) is a ubiquitous cytosolic protein from the class II HDACs family with X-linked inheritance, that binds to and deacetylates α-tubulin at Lys40 (Hubbert et al., 2002; Valenzuela-Fernandez et al., 2008). HDAC6 also modulates other substrates, for example, cortactin and Hsp90. HDAC6 controls cell migration (Zhang et al., 2007), T-regulatory functions (de Zoeten et al., 2011) and CD4$^+$ T cell activation (Serrador et al., 2004). Consistent with this, HDACs inhibitors impair some immune functions (Mosley et al., 2006; Tsuji et al., 2015). However, the precise contribution *in vivo* (by using *Hdac6*$^{-/-}$ mice) has not been assessed, and the mechanisms involved remain unsolved. HDAC6 also functions as a scaffold protein in T cell migration (Cabrero et al., 2006) and the transport of misfolded proteins (Kawaguchi et al., 2003). In this report, we describe the impaired killing capacity of *Hdac6*$^{-/-}$ CTLs. The molecular mechanism underlying this defect involves a scaffold role that positions HDAC6 as a protein that oversees the proper movement of lytic granules, their transport to the immune synapse and secretion towards the target cell.

RESULTS AND DISCUSSION

HDAC6 deficiency reduces the cytolytic capacity of CD8$^+$ T lymphocytes

We examined the ability of cytotoxic T cells from *Hdac6*$^{-/-}$ mice to kill target cells *in vitro*. CD8$^+$ T cells from wild-type (WT) and *Hdac6*$^{-/-}$ mice expressing the transgenic ovalbumin (OVA)-specific TCR (OT-I) were activated *in vitro* and cultured to generate CTLs. Cell cytotoxicity was subsequently analyzed by survival of dye-labeled EL4 target cells pulsed or not with $OVA_{257–264}$ peptide (SIINFEKL). *Hdac6*$^{-/-}$ CTLs showed decreased killing activity (Fig. 1A), consistent with reduced expression of CD107a (also known as LAMP1) in *Hdac6*$^{-/-}$ CTLs upon degranulation (Fig. 1B). Likewise, CTLs from OT-I mice treated with tubastatin A, a potent HDAC6 inhibitor (Butler et al., 2010), displayed a reduced killing ability (Fig. S1A). We also detected decreased Prf1 secretion from activated (i.e. induced by anti-CD3 and anti-CD28 monoclonal antibodies) *Hdac6*$^{-/-}$ CTLs (Fig. 1C, left). Next, we assessed the secretion promoted by phorbol-12-myristate-13-acetate (PMA), to bypass TCR stimulation. Both cathepsin D and Prf1 decreased in supernatants from activated *Hdac6*$^{-/-}$ CTLs (Fig. 1C, right). Taken together, our data demonstrate that *Hdac6*$^{-/-}$ CTLs show reduced cytotoxic activity and suggest that HDAC6 controls exocytosis.

[1]Servicio de Inmunología, Hospital Universitario de la Princesa, UAM, IIS-IP, Madrid 28006, Spain. [2]Laboratory of Intercellular communication, Fundación CNIC, Madrid 28029, Spain. [3]Immunobiology of inflammation, Fundación CNIC, Madrid 28029, Spain. [4]Microscopy and Dynamic Imaging Unit, Fundación CNIC, Madrid 28029, Spain. [5]Spettroscopia biomedica in fluorescenza dinamica, Center of Experimental Imaging, Ospedale San Raffaele, Milan 20132, Italy. [6]Proteomic Unit, Fundación CNIC, Madrid 28029, Spain. [7]Dept. Biochemistry and Molecular and Cell Biology, Universidad de Zaragoza, Zaragoza 50009, Spain. [8]Laboratory of Normal and Pathological Homeostasis of the Immune System, INSERM Unité Mixte de Recherche, Paris 1163, France. [9]Department of Pharmacology and Cancer Biology Duke University, Medical Center, Durham, NC 27710, USA.
*These authors contributed equally to this work

‡Author for correspondence (fsmadrid@salud.madrid.org)

Received 22 September 2015; Accepted 8 February 2016

Journal of Cell Science (2016) 129, 1305-1311 doi:10.1242/jcs.180885

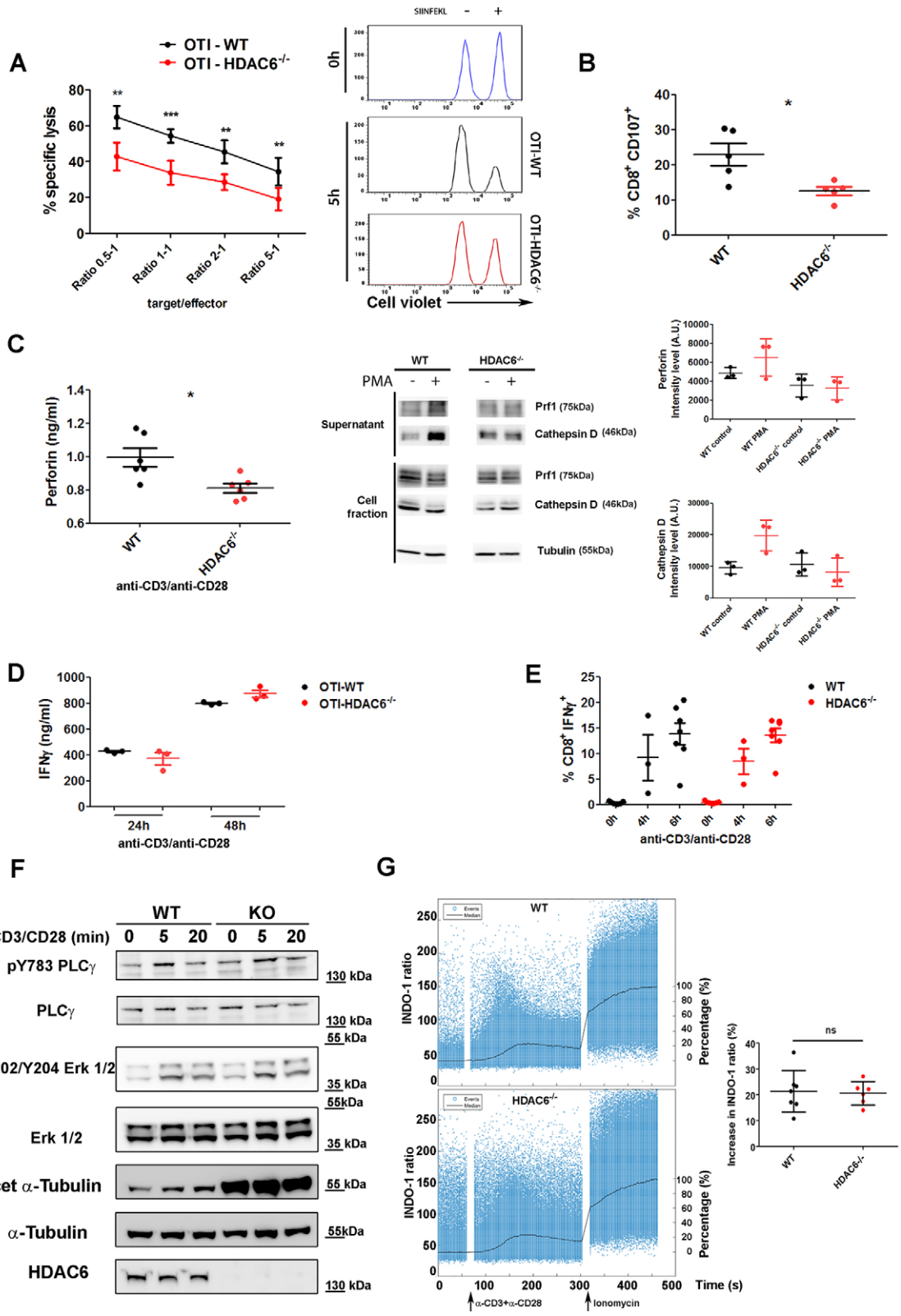

Fig. 1. See next page for legend.

We next tested IFN-γ production; the frequency of CTLs producing IFNγ and its secretion was unaffected in activated *Hdac6*$^{-/-}$ CTLs (Fig. 1D,E), in contrast to what has been described for ACY-1215, a recently described inhibitor that is tenfold more selective for HDAC6 than for HDAC1, HDAC2 and HDAC3 (class I HDACs) that shows slight activity against HDAC8 (Tsuji et al., 2015). Likewise, treatment of CTLs from OT-I mice with tubastatin A had no significant effect (Fig. S1B). Importantly, T cell signaling induced by anti-CD3 and anti-CD28 monoclonal antibodies in *Hdac6*$^{-/-}$ cells was comparable to control, as determined by

Journal of Cell Science (2016) 129, 1305-1311 doi:10.1242/jcs.180885

Fig. 1. HDAC6 modulates the efficiency of target cell killing and degranulation of lytic mediators. (A) Graph showing *in vitro* cytotoxic assay for specific lysis of SIINFEKL-pulsed EL4 target cells by OT-I (OTI) WT or *Hdac6*$^{-/-}$ CTLs. Mean±s.e.m. (n=5 mice for each genotype) of specific lysis for 5 h are shown at the indicated target to effector ratios. All killing assays were performed in triplicate. **P<0.01; ***P<0.001 (unpaired t-test). Histograms show a representative FACS profile. (B) Degranulation is shown as the percentage of CD107a^{+} cells detected by FACS in activated versus non-stimulated WT and *Hdac6*$^{-/-}$ CD8^{+} CTLs. Results are mean±s.e.m.; n=5 for each genotype. *P<0.05 (unpaired t-test). (C) Exocytosis of lytic mediators upon T cell activation. Left, perforin content in culture cell supernatants as determined by ELISA. CTLs were stimulated with anti-CD3, and anti-CD28 monoclonal antibodies and goat anti-Armenian-hamster IgG antibodies (5 h). Graphs show mean±s.e.m. (n=6 mice for each genotype). *P<0.05 (unpaired t-test). Middle panel, representative western blot showing exocytosis. PMA stimulation was for 1 h. Normalization was performed against cell fractions. Right graphs, quantification of the experiments (mean±s.e.m.; three independent experiments). (D) IFNγ secretion in supernatants from WT and *Hdac6*$^{-/-}$ CTLs activated by anti-CD3 and anti-CD28 monoclonal antibodies as determined by ELISA. Results are mean±s.e.m.; n=3 for each genotype; Mann–Whitney test. (E) Percentage of IFNγ^{+} cells in WT and *Hdac6*$^{-/-}$ CTLs activated by activated by anti-CD3 and anti-CD28 monoclonal antibodies. Results are mean±s.e.m.; n=6 (0 and 6 h) and n= 3 (4 h) for each genotype; Mann–Whitney test. (F) Effector CD8^{+} CTLs isolated from WT and *Hdac6*$^{-/-}$ mice were activated (by anti-CD3 and anti-CD28 monoclonal antibodies), lysed and blotted for PLCγ (pY783) and Erk1/2 (pT202/Y204) phosphorylation, and tubulin acetylation (acet). (G) Ca^{2+} flux. WT and *Hdac6*$^{-/-}$-purified CTLs pre-loaded with the INDO-1 AM probe were analyzed for free and bound Ca^{2+} by flow cytometry. Left graphs, time course of ratiometric variation (left y axis); black line, median activation as normalized to basal levels (0%) and total activation by ionomycin treatment (100%; right y axis). Stimuli are indicated. A representative experiment is shown. Right graph, mean±s.d. of the increase in the ratio (WT, n=7; *Hdac6*$^{-/-}$, n=6). ns, not significant (Mann–Whitney test).

assessing PLCγ1 and Erk1 and Erk2 (Erk1/2; also known as MAPK3 and MAPK1, respectively) phosphorylation (Fig. 1F). Likewise, the increase in intracellular Ca^{2+} remained unchanged upon activation (Fig. 1G). As expected, tubulin acetylation at Lys40 was increased in *Hdac6*$^{-/-}$ CTLs (Fig. 1F). These results suggest that the killing defect observed does not result from a general impairment of CTLs function.

Defective *in vivo* and *ex vivo* killing in HDAC6-knockout mice

The effector activity of *Hdac6*$^{-/-}$ CD8^{+} T cells was tested *in vivo* following immunization of mice by inoculation with SIINFEKL-pulsed dendritic cells. The *in vivo* killing activity against the injected splenocytes as target cells (pulsed or not with SIINFEKL) was analyzed upon recovery by peritoneal lavage. Notably, *Hdac6*$^{-/-}$ mice showed reduced specific killing of target cells (Fig. 2A, left panel). However, the proportion of SIINFEKL-specific CD8^{+} T cells in the endogenous repertoire was not affected in *Hdac6*$^{-/-}$ mice (Fig. 2A, right panel), suggesting that the cytotoxic function rather than the number of antigen-specific CTLs could underlie the defect. Next, we examined whether the decreased cytotoxic function of the CTLs resulted in an impaired ability to prevent morbidity and/or mortality during a viral infection. To restrict HDAC6 deficiency to CD8^{+} T cells, we adoptively transferred *Rag1*$^{-/-}$ mice with WT or *Hdac6*$^{-/-}$ naïve CD8^{+} T cells and subsequently challenged with a fully replicative vaccinia virus (VACV) WR strain. This infection model mimics the immunological and clinical features of smallpox vaccination in humans (Mota et al., 2011). CD8^{+} T cell proliferation was comparable, or even increased (division 4) in *Hdac6*$^{-/-}$ mice (Fig. 2B). *Rag1*$^{-/-}$ mice adoptively transferred with *Hdac6*$^{-/-}$ CD8^{+} T cells showed increased morbidity at 9 and 11 days post-infection (dpi) (Fig. 2C). Virus titration from the lesion tissue demonstrated that *Hdac6*$^{-/-}$ immune cells exerted a less-efficient virus clearance (Fig. 2D). Consistent with our findings on the lack of effect in endogenous antigen-specific CD8^{+} T cell numbers, CTL expansion tracked at 13 dpi was not affected in *Hdac6*$^{-/-}$ mice (Fig. 2E, left). The proportion of activated CD8^{+} T cells (CD44high, with high expression of CD44) at early (5 dpi) and late stages (13–30 dpi) of the disease were similar for WT and *Hdac6*$^{-/-}$ mice (tested in peripheral blood and spleen, respectively; Fig. 2E, right). These *in vivo* results emphasize the role of HDAC6 in the CD8+ T-cell-dependent protection against VACV infection without affecting effector CD8^{+} CTL differentiation.

HDAC6 drives the terminal transport of lytic granules to the target cell

CTL killing is limited to target cells (and not neighbor cells) by the confinement of secretion to the immune synapse established between the CTL and the target cell (de Saint Basile et al., 2010). Interestingly, the intracellular colocalization between cathepsin D and Lamp1 (CD107a) was affected in *Hdac6*$^{-/-}$ CTLs conjugated with target cells, pointing to the mislocalization of lytic mediators in these cells (Fig. 3A; images and middle graphs). The decreased secretion of lytic proteins from *Hdac6*$^{-/-}$ CTLs suggests that HDAC6 regulates exocytosis of lytic granules (Fig. 1C). Indeed, the translocation of the centrosome to the contact area with the target cell was more pronounced in *Hdac6*$^{-/-}$ CTLs than in WT cells (Fig. 3A, right graph), in accordance with the effect described for the HDAC inhibitor Trichostatin A on the centrosomal polarization in CD4^{+} T cells (Serrador et al., 2004). This suggests that the defective exocytosis might rely on the movement of lytic granules themselves.

We thus monitored the dynamics of lytic granules at the subcortical immune synapse cytoskeleton and their release by total internal reflection fluorescence microscopy (TIRFm). CTLs were loaded with a pH-dependent lysosomal tracker, which allows the visualization of the lytic granules, and settled on to a stimulating surface to form an immune-synapse-like structure (Fig. 3B). These experiments revealed significant changes in the distribution of the lytic granules and their dynamics, with a marked decrease in the number of lytic granules detected at the immune-synapse-like structure in *Hdac6*$^{-/-}$ cells, suggesting alterations to the active transport of the granules from the centrosomal region to the plasma membrane. Indeed, the mean fluorescence intensity detected for *Hdac6*$^{-/-}$ granules was lower, which suggests a higher pH and, therefore, a different degree of maturation, although the lytic granules displayed similar sizes in WT and *Hdac6*$^{-/-}$ cells (Fig. 3C). The most remarkable difference pertained to the x–y distribution of the lytic granules, which was wider (diffusion surface) in the *Hdac6*$^{-/-}$ CTLs, with a higher diffusion coefficient, although there were similar duration times and path lengths (Fig. 3D). These data suggest that the lytic granules from *Hdac6*$^{-/-}$ CTLs are not properly targeted and/or that they dock inefficiently at the immune synapse.

Tubulin motors control the delivery of lytic granules to the plasma membrane. Whereas dynein controls lytic granule targeting to the centrosome (Burkhardt et al., 1993; Mentlik et al., 2010), the kinesin-1–Slp3–Rab27a (Slp3 is also known as SYTL3) complex directs terminal transport to the plasma membrane for exocytosis (Kurowska et al., 2012). Dynactin might also be part of this complex, linking the cargo to kinesin-1 motor (Haghnia et al., 2007; Hendricks et al., 2010). We then hypothesized that HDAC6 regulates the movement and delivery of the lytic granules at the immune synapse through kinesin-1. Using a biochemical approach, we observed that HDAC6 formed a complex with kinesin-1 light chain (KLC1) upon triggering

Journal of Cell Science (2016) 129, 1305-1311 doi:10.1242/jcs.180885

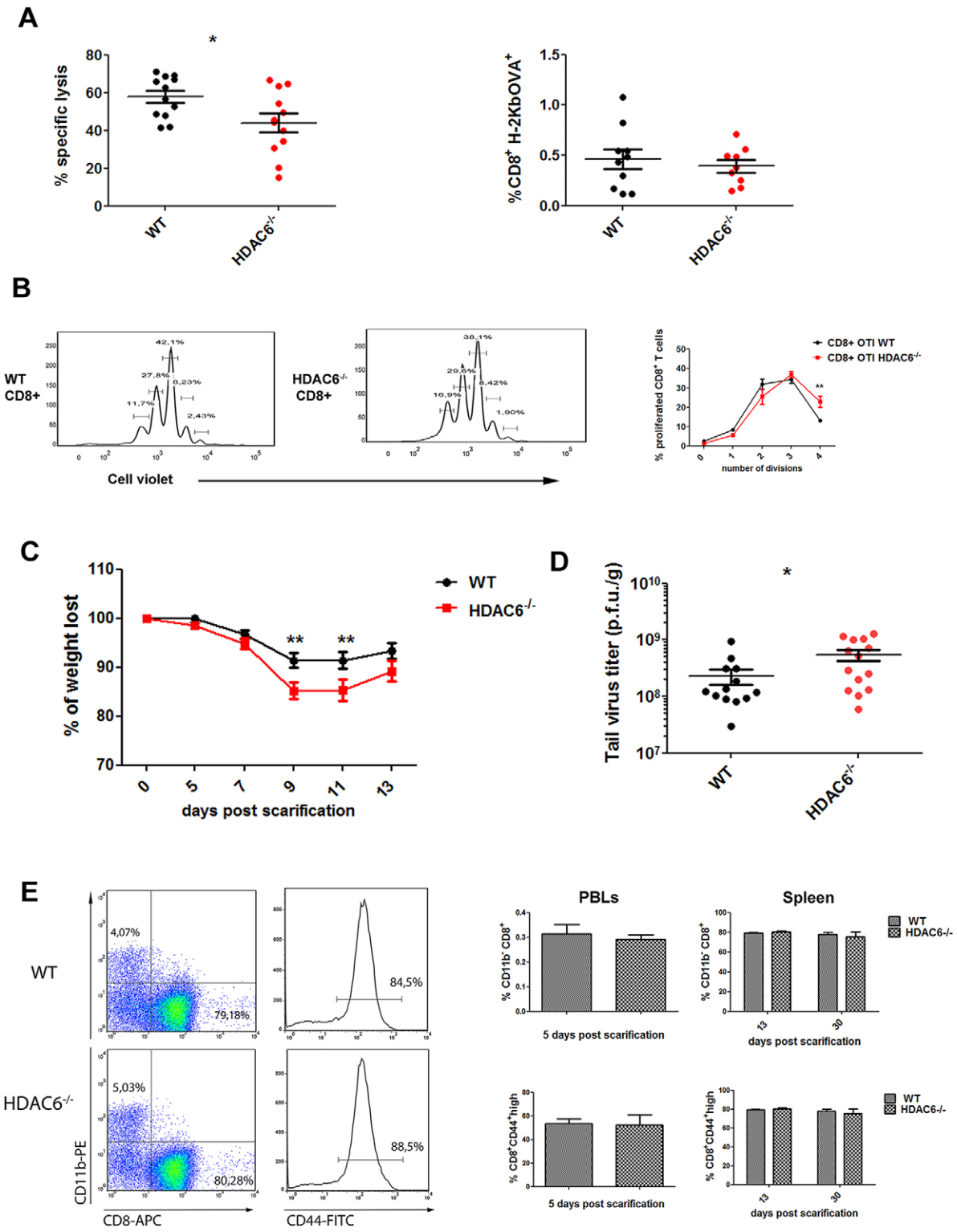

Fig. 2. *In vivo* function of CTLs is impaired in HDAC6 knockout mice. (A) WT and *Hdac6*$^{-/-}$ were immunized against SIINFEKL peptide. 7 days after immunization, Cell-Violet-labeled target cells that had been SIINFEKL-pulsed (1 µM) or not were injected intraperitoneally, and recovered through intraperitoneal lavage (24 h). Cell survival assessed by FACS (left panel). Data represent mean±s.e.m. n=12 for each genotype from three independent experiments. *P<0.05, Mann–Whitney test. The relative percentage of CD8$^+$ H-2Kb$^+$ cells was determined to control avidity towards SIINFEKL (right panel, results are mean±s.e.m.; WT, n=10; *Hdac6*$^{-/-}$, n=9 from three independent experiments; Mann–Whitney test.) (B) Proliferation of CD8$^+$ cells in VACV-OVA-infected WT and *Hdac6*$^{-/-}$ mice. Results are means±s.e.m. (n=5 for each genotype); **P<0.01 (Mann–Whitney test). (C) *Rag1*$^{-/-}$ mice inoculated intravenously with 0.8×10^6 CD8$^+$ naïve cells and infected with VACV-WR through tail scarification were weighed every 2 days. Results are means±s.e.m. (n=10 for each genotype). **P<0.01 (Mann–Whitney test). (D) Titration of viral particles from scarified tails (13 dpi). The colonies of CV-1 cells infected *in vitro* with different dilutions of tail extracts were counted, and normalized to the tail tissue weight. Results are means±s.e.m. (WT, n=13; *Hdac6*$^{-/-}$, n=14); *P<0.05 (Mann–Whitney test). (E) Percentage of CD8$^+$ expansion and CD44 expression by FACS analysis in peripheral blood (5 dpi) and in spleen populations (13 and 30 dpi). CD11b was used as negative control. Results are means±s.e.m. (n=5; Mann–Whitney test).

Journal of Cell Science (2016) 129, 1305-1311 doi:10.1242/jcs.180885

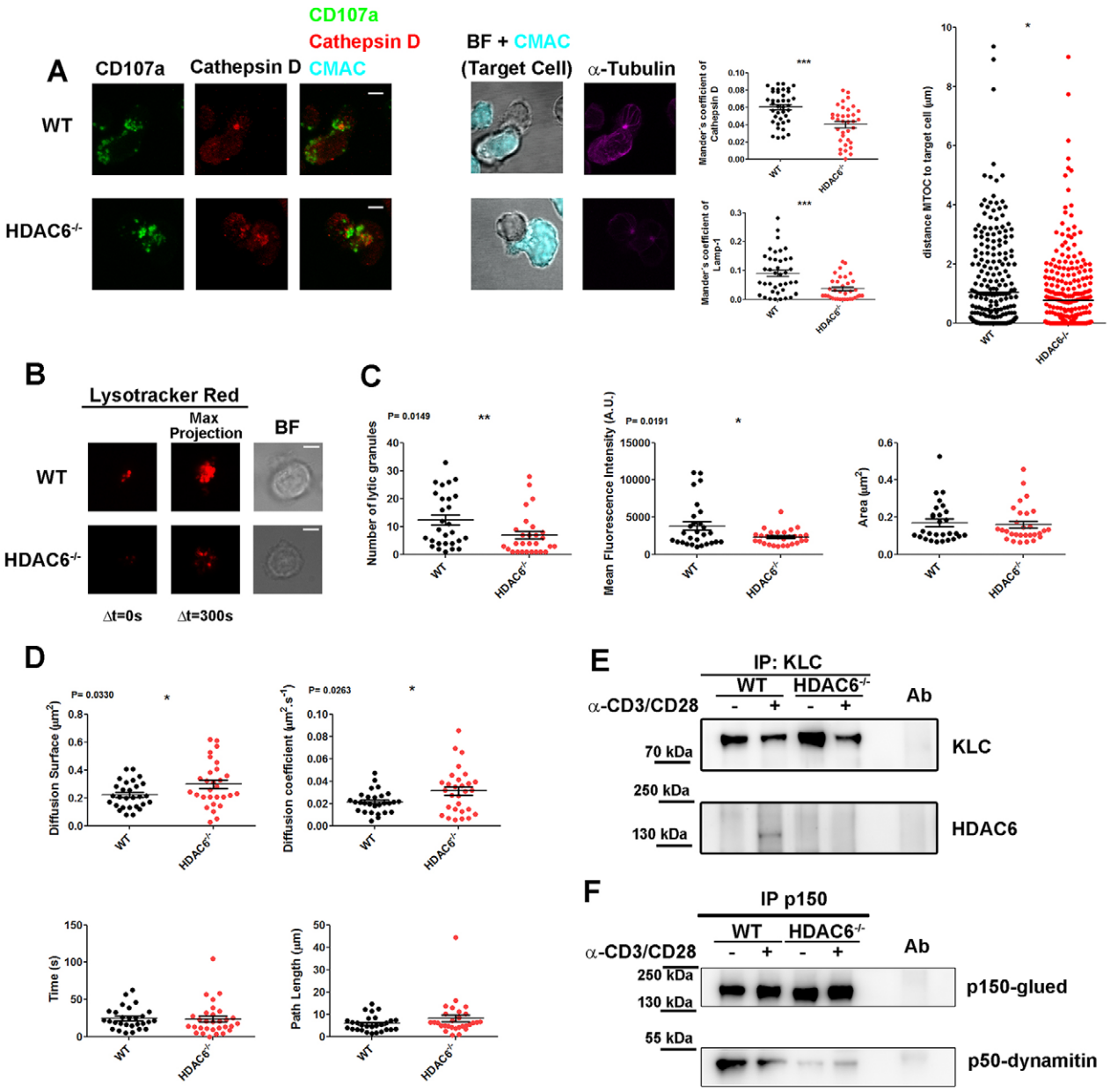

Fig. 3. HDAC6 drives the terminal transport of lytic granules to the target cell. (A) Confocal microscopy images of WT and *Hdac6*$^{-/-}$ OT-I-derived CTLs conjugated with 7-amino-4-chloromethylcoumarin (CMAC)-loaded, OVA-pre-pulsed target EL4 cell (500 nM SIINFEKL, cyan) for 15 min. Green, CD107a; red, cathepsin D; magenta, α-tubulin. Bright-field (BF) images correspond to a unique plane, and fluorescence images correspond to maximal projections from *z*-stacks. Middle graphs, Manders' coefficient for colocalization of Lamp1 and cathepsin D. Results are mean±s.e.m. (WT, *n*=39; *Hdac6*$^{-/-}$, *n*=35). ***P<0.001 (Mann–Whitney test). Right graph, quantification (mean) of microtubule-organizing center (MTOC) translocation (*n*>270, from three independent experiments). *P<0.05 (unpaired *t*-test). (B) Representative TIRFm images of Lysotracker-Red-loaded WT and *Hdac6*$^{-/-}$ CTLs in glass-bottom chambers coated with anti-CD3 and anti-CD28 monoclonal antibodies. Video recording was initiated upon cell adhesion (37°C and 5% CO_2). Images were acquired for 5 min every 0.5 s. (C,D) Quantification for lytic granules parameters at the immune-synapse-like structure was performed for each cell (*n*=28 for each genotype, three independent experiments). Results are mean±s.e.m. (*n*=28 for each genotype). *P<0.05; **P<0.01 (Mann–Whitney). (E,F) Western blots showing immunoprecipitates (IP) from resting or activated WT and *Hdac6*$^{-/-}$ CTLs (15 min) from a representative experiment out of three. Anti-KLC1 (E) or anti-p150 glued (p150) antibodies were used (F). Samples were blotted against indicated antibodies. Ab, pre-immune control antibody. Scale bars: 4 µm.

with anti-CD3 and anti-CD28 monoclonal antibodies (Fig. 3E). Moreover, interaction of the kinesin-activator complex dynactin subunits p150-glued (also known as DCTN1) and p50-dynamitin (also known as DCTN2) was impaired in *Hdac6*$^{-/-}$ (Fig. 3F).

In summary, our data support a specific role for HDAC6 in the intracellular localization of lytic mediators and, particularly, in their exocytosis. Therefore, the catalytic and scaffold activities of HDAC6 might act at multiple levels in the control of cytotoxic-related pathways, making HDAC6 a potential candidate that could be targeted to modulate CTLs in specific diseases.

MATERIALS AND METHODS

Mice

Hdac6$^{-/-}$ mice were generated through targeting of exons 10 to 13 (Gao et al., 2007). They were intercrossed in a C57BL/6 background to generate wild-type and knockout littermates. Mice presenting transgenic inserts for mouse

Tcra-Variable2 and Tcrb-Variable5 genes, which TCR recognizes ovalbumin$_{257-264}$ peptide in the context of H2Kb MHC-I (OT-I) were crossed to female *Hdac6*$^{+/-}$mice to generate WT and KO littermates; males were used for *in vivo* experimentation given that *Hdac6* is an X-linked gene. *Rag1*$^{-/-}$ mice were used for adoptive transfer experiments. These studies were approved by the local Ethics Committee for Basic Research at the CNIC and the Comunidad Autónoma de Madrid.

Cell culture

Cytotoxic cells were produced by culturing cells upon stimulation with SIINFEKL peptide (0.5 µM, 24 h) or concanavalin A (2.5 µg/ml, 36 h) and cultured in presence of IL-2 (50–100 IU/ml) for at least 7 days. All other cells were cultured and treated as described previously (Cascio et al., 2015; Martín-Cófreces et al., 2006; Sancho et al., 2008).

Immunoprecipitation, CTL signaling and immunoblotting

Experiments were performed as described previously (Martín-Cófreces et al., 2012, 2008, 2006); anti-KLC1 antibody was from Merck Millipore (Darmstadt, Germany; KLC; at 5 µg/ml for immunoprecipitation and 1 µg/ml for western blotting), anti-HDAC6 (at 0.1 µg/ml for western blotting) from Assay Biotech (Sunnyvale, CA), and anti-p50 and -p150 from BD Pharmingen (Franklin Lakes, New Jersey, US; anti-p150 was used at 1 µg/ml for immunoprecipitation and 0.25 µg/ml for western blotting. Anti-p50 at 0.25 µg/ml for western blotting).

Measurement of intracellular variations in Ca^{2+} levels by using flow cytometry

The method used for intracellular Ca^{2+} influx has been described previously (June and Moore, 2004). In particular, 5×10^6 purified $CD8^+$ CTLs generated *in vitro* were loaded with 2 µg ml^{-1} INDO-1 AM (Invitrogen Corporation) and stimulated with anti-CD3 and anti-CD28 monoclonal antibodies (BD Biosciences; Franklin Lakes, NJ) plus goat anti-Armenian-hamster IgG antibodies (Jackson Immunoresearch Laboratories; West Grove, PA; 6, 3 and 6 µg/ml, respectively).

In vitro degranulation assay

CD107a expression was monitored with Alexa-Fluor-647-conjugated anti-CD107a antibody (BD Biosciences) in monensin-pretreated $CD8^+$ OT-I cells (5 mM) stimulated with SIINFEKL-pulsed (1 µM; 3 h, 37°C) EL4 cells. Cells were stained with phycoerythrin-conjugated anti-CD8 and FITC-conjugated anti-CD44 antibody, analyzed by fluorescence-activated cell sorting (FACS) and data were processed with FlowJo 7.6.5 (TreeStar Inc, Ashland, OR).

Confocal and total internal reflection fluorescence microscopy analysis

Cell conjugates between CTLs and EL4 cells were allowed to form (15 min) and processed as described previously (Cascio et al., 2015; Martín-Cófreces et al., 2006) under a Leica SP5 confocal microscope (Leica Microsystems; Mannheim, Germany) mounted on an inverted DMI6000 microscope fitted with a HCX PL APO 63×1.40-0.6 NA oil objective. Images were processed using Imaris software (Bitplane; Zurich, Switzerland) and Image J software (http://rsbweb.nih.gov/ij/), and assembled with Photoshop 6 software. The 3D distance from the centrosomal center of mass to the target cell-edge was measured by generating image masks from fluorescence with Imaris Software. TIRFm imaging was performed with a Leica AM-TIRF-MC-M system mounted on a Leica DMI-6000B microscope coupled to an Andor-DU8285_VP-4094 camera (Andor; Belfast, UK) fitted with a HCX-PL-APO 100.0×1.46 NA oil objective as described previously (Baixauli et al., 2011; Martín-Cófreces et al., 2012). The laser penetrance used was 90 nm (561 nm laser). The mechanical properties of the lytic granules were determined with a user-customized routine developed in Python. The software can be freely downloaded from: https://dl.dropboxusercontent.com/u/4050954/VesiclesAnalyser.zip. For more information, see the tutorial included.

Vaccinia virus infection and virus titration

Tails were scarified with vaccinia virus [VACV; 2×10^6 plaque-forming units (PFU)/mouse] by gently scratching (×25) with a 28 1/2 G needle. For virus titration, tails were mechanical disaggregated (1 ml of PBS), subjected to freeze-thaw cycles and sonication. Serial dilutions of the homogenates were added to monolayers of CV-1 cells seeded in 24-well plates. Cells were stained with Cristal Violet 24 h later. We observed a detection limit of 5 PFU/tail, the number of plaques was multiplied by the reciprocal of sample dilution and converted to PFU/g of tissue.

In vitro and *in vivo* cytotoxicity assay

For *in vitro* experiments, EL4 target cells were incubated with 1 µM Cell Violet and pulsed with 1 µM SIINFEKL, or with 0.1 µM Cell Violet and no SIINFEKL, washed extensively, mixed (1:1), pooled with different dilutions of effectors, plated in a 96-well U-bottomed plate for 5 h (37°C) in triplicate and analyzed by FACS. Dead cells were excluded on the basis of propidium iodide staining. The mean percentage of survival in antigen-loaded targets was calculated relative to antigen-negative internal controls in each sample. Specific lysis was calculated by using the following equation: percentage specific lysis=100×[1−(percentage of cells staining for Cell Violet at 1 µM/percentage of cells staining for Cell Violet at 0.1 µM)]. All data were normalized to the basal specific lysis in absence of effector cells. For *in vivo* assays, WT and *Hdac6*$^{-/-}$ mice were inoculated by intraperitoneal injection of bone marrow dendritic cells pulsed with 1 µM of SIINFEKL and lipopolysaccharide (LPS; 1 µg ml^{-1}) for 1 h. After 7 days, CD45.1 splenocytes were prepared as targets as described above and injected intraperitoneally into recipients. Cells were recovered 24 h later by peritoneal lavage and *in vivo* killing levels measured (Hermans et al., 2004; Iborra et al., 2012; Sancho et al., 2008; Schulz et al., 2005).

Statistical analysis

Data were analyzed with GraphPad Prism software (La Jolla, CA) for normality (D'Agostino-Pearson or the Kolmogorov–Smirnov test for small samples). Student's *t*-tests or Mann–Whitney tests were used for normal or non-normal data, respectively, and two-tailed ANOVA for grouped data (Bonferroni post-test).

Acknowledgements

We thank Manuel Gomez and Miguel Vicente for critical reading of the manuscript. Experimentation was performed at Cellomics and Microscopy Units (CNIC) and Flow Cytometry Core Unit (CNIO).

Competing interests

The authors declare no competing or financial interests.

Author contributions

N.N.-A., N.B.M.-C. and F.S.-M. designed experiments, made the figures and wrote the manuscript; N.N.A., S.I., N.B.M.-C., O.M.-G., J.V., D.S., G.M. and T.-P.Y. and E.C. collected and/or analyzed data; A.T. developed the Quant Application.

Funding

This work was supported by the Ministerio de Economía y competitividad (MINECO) [grant number SAF2014-55579-R]; Comunidad Autónoma de Madrid (CAM) [grant number INDISNET01592006]; Instituto de Salud Carlos III y Fondo Europeo de Desarrollo Regional (FEDER) [grant numbers BIOMID-PIE13/041 and RD12/0042/0056]; European Research Council (ERC) [grant number ERC-2011-AdG 294340-GENTRIS]. The Centro Nacional de Investigaciones Cardiovasculares (CNIC) is supported by the MINECO and Pro-CNIC Foundation.

Supplementary information

Supplementary information available online at
http://jcs.biologists.org/lookup/suppl/doi:10.1242/jcs.180885/-/DC1

References

Baixauli, F., Martín-Cófreces, N. B., Morlino, G., Carrasco, Y. R., Calabia-Linares, C., Veiga, E., Serrador, J. M. and Sánchez-Madrid, F. (2011). The mitochondrial fission factor dynamin-related protein 1 modulates T-cell receptor signalling at the immune synapse. *EMBO J.* **30**, 1238-1250.

Burkhardt, J. K., McIlvain, J. M., Jr., Sheetz, M. P. and Argon, Y. (1993). Lytic granules from cytotoxic T cells exhibit kinesin-dependent motility on microtubules in vitro. *J. Cell Sci.* **104**, 151-162.

Butler, K. V., Kalin, J., Brochier, C., Vistoli, G., Langley, B. and Kozikowski, A. P. (2010). Rational design and simple chemistry yield a superior, neuroprotective HDAC6 inhibitor, tubastatin A. *J. Am. Chem. Soc.* **132**, 10842-10846.

Cabrero, J. R., Serrador, J. M., Barreiro, O., Mittelbrunn, M., Naranjo-Suárez, S., Martín-Cófreces, N., Vicente-Manzanares, M., Mazitschek, R., Bradner, J. E., Ávila, J. et al. (2006). Lymphocyte chemotaxis is regulated by histone deacetylase 6, independently of its deacetylase activity. *Mol. Biol. Cell* **17**, 3435-3445.

Cascio, G., Martin-Cofreces, N. B., Rodriguez-Frade, J. M., Lopez-Cotarelo, P., Criado, G., Pablos, J. L., Rodriguez-Fernandez, J. L., Sanchez-Madrid, F. and Mellado, M. (2015). CXCL12 regulates through JAK1 and JAK2 formation of productive immunological synapses. *J. Immunol.* **194**, 5509-5519.

de Saint Basile, G., Ménasché, G. and Fischer, A. (2010). Molecular mechanisms of biogenesis and exocytosis of cytotoxic granules. *Nat. Rev. Immunol.* **10**, 568-579.

de Zoeten, E. F., Wang, L., Butler, K., Beier, U. H., Akimova, T., Sai, H., Bradner, J. E., Mazitschek, R., Kozikowski, A. P., Matthias, P. et al. (2011). Histone deacetylase 6 and heat shock protein 90 control the functions of Foxp3(+) T-regulatory cells. *Mol. Cell. Biol.* **31**, 2066-2078.

Gao, Y.-s., Hubbert, C. C., Lu, J., Lee, Y.-S., Lee, J.-Y. and Yao, T.-P. (2007). Histone deacetylase 6 regulates growth factor-induced actin remodeling and endocytosis. *Mol. Cell. Biol.* **27**, 8637-8647.

Haghnia, M., Cavalli, V., Shah, S. B., Schimmelpfeng, K., Brusch, R., Yang, G., Herrera, C., Pilling, A. and Goldstein, L. S. (2007). Dynactin is required for coordinated bidirectional motility, but not for dynein membrane attachment. *Mol. Biol. Cell* **18**, 2081-2089.

Hendricks, A. G., Perlson, E., Ross, J. L., Schroeder, H. W., III, Tokito, M. and Holzbaur, E. L. F. (2010). Motor coordination via a tug-of-war mechanism drives bidirectional vesicle transport. *Curr. Biol.* **20**, 697-702.

Hermans, I. F., Silk, J. D., Yang, J., Palmowski, M. J., Gileadi, U., McCarthy, C., Salio, M., Ronchese, F. and Cerundolo, V. (2004). The VITAL assay: a versatile fluorometric technique for assessing CTL- and NKT-mediated cytotoxicity against multiple targets in vitro and in vivo. *J. Immunol. Methods* **285**, 25-40.

Hubbert, C., Guardiola, A., Shao, R., Kawaguchi, Y., Ito, A., Nixon, A., Yoshida, M., Wang, X.-F. and Yao, T.-P. (2002). HDAC6 is a microtubule-associated deacetylase. *Nature* **417**, 455-458.

Iborra, S., Izquierdo, H. M., Martínez-López, M., Blanco-Menéndez, N., Reis e Sousa, C. and Sancho, D. (2012). The DC receptor DNGR-1 mediates cross-priming of CTLs during vaccinia virus infection in mice. *J. Clin. Invest.* **122**, 1628-1643.

June, C. H. and Moore, J. S. (2004). Measurement of intracellular ions by flow cytometry. *Curr. Protoc. Immunol.* Chapter 5, Unit 5 5.

Kawaguchi, Y., Kovacs, J. J., McLaurin, A., Vance, J. M., Ito, A. and Yao, T.-P. (2003). The deacetylase HDAC6 regulates aggresome formation and cell viability in response to misfolded protein stress. *Cell* **115**, 727-738.

Kurowska, M., Goudin, N., Nehme, N. T., Court, M., Garin, J., Fischer, A., de Saint Basile, G. and Menasche, G. (2012). Terminal transport of lytic granules to the immune synapse is mediated by the kinesin-1/Slp3/Rab27a complex. *Blood* **119**, 3879-3889.

Lopez, J. A., Jenkins, M. R., Rudd-Schmidt, J. A., Brennan, A. J., Danne, J. C., Mannering, S. I., Trapani, J. A. and Voskoboinik, I. (2013). Rapid and unidirectional perforin pore delivery at the cytotoxic immune synapse. *J. Immunol.* **191**, 2328-2334.

Martín-Cófreces, N. B., Sancho, D., Fernandez, E., Vicente-Manzanares, M., Gordon-Alonso, M., Montoya, M. C., Michel, F., Acuto, O., Alarcon, B. and Sanchez-Madrid, F. (2006). Role of Fyn in the rearrangement of tubulin cytoskeleton induced through TCR. *J. Immunol.* **176**, 4201-4207.

Martín-Cófreces, N. B., Robles-Valero, J., Cabrero, J. R., Mittelbrunn, M., Gordon-Alonso, M., Sung, C.-H., Alarcon, B., Vazquez, J. and Sanchez-Madrid, F. (2008). MTOC translocation modulates IS formation and controls sustained T cell signaling. *J. Cell Biol.* **182**, 951-962.

Martín-Cófreces, N. B., Baixauli, F., Lopez, M. J., Gil, D., Monjas, A., Alarcon, B. and Sanchez-Madrid, F. (2012). End-binding protein 1 controls signal propagation from the T cell receptor. *EMBO J.* **31**, 4140-4152.

Mentlik, A. N., Sanborn, K. B., Holzbaur, E. L. and Orange, J. S. (2010). Rapid lytic granule convergence to the MTOC in natural killer cells is dependent on dynein but not cytolytic commitment. *Mol. Biol. Cell* **21**, 2241-2256.

Mosley, A. J., Meekings, K. N., McCarthy, C., Shepherd, D., Cerundolo, V., Mazitschek, R., Tanaka, Y., Taylor, G. P. and Bangham, C. R. (2006). Histone deacetylase inhibitors increase virus gene expression but decrease CD8+ cell antiviral function in HTLV-1 infection. *Blood* **108**, 3801-3807.

Mota, B. E. F., Gallardo-Romero, N., Trindade, G., Keckler, M. S., Karem, K., Carroll, D., Campos, M. A., Vieira, L. Q., da Fonseca, F. G., Ferreira, P. C. P. et al. (2011). Adverse events post smallpox-vaccination: insights from tail scarification infection in mice with Vaccinia virus. *PLoS ONE* **6**, e18924.

Pardo, J., Aguilo, J. I., Anel, A., Martin, P., Joeckel, L., Borner, C., Wallich, R., Müllbacher, A., Froelich, C. J. and Simon, M. M. (2009). The biology of cytotoxic cell granule exocytosis pathway: granzymes have evolved to induce cell death and inflammation. *Microbes Infect.* **11**, 452-459.

Ritter, A. T., Angus, K. L. and Griffiths, G. M. (2013). The role of the cytoskeleton at the immunological synapse. *Immunol. Rev.* **256**, 107-117.

Sancho, D., Mourão-Sá, D., Joffre, O. P., Schulz, O., Rogers, N. C., Pennington, D. J., Carlyle, J. R. and Reis e Sousa, C. (2008). Tumor therapy in mice via antigen targeting to a novel, DC-restricted C-type lectin. *J. Clin. Invest.* **118**, 2098-2110.

Schulz, O., Diebold, S. S., Chen, M., Näslund, T. I., Nolte, M. A., Alexopoulou, L., Azuma, Y.-T., Flavell, R. A., Liljeström, P. and Reis e Sousa, C. (2005). Toll-like receptor 3 promotes cross-priming to virus-infected cells. *Nature* **433**, 887-892.

Serrador, J. M., Cabrero, J. R., Sancho, D., Mittelbrunn, M., Urzainqui, A. and Sánchez-Madrid, F. (2004). HDAC6 deacetylase activity links the tubulin cytoskeleton with immune synapse organization. *Immunity* **20**, 417-428.

Tsuji, G., Okiyama, N., Villarroel, V. A. and Katz, S. I. (2015). Histone deacetylase 6 inhibition impairs effector CD8 T-cell functions during skin inflammation. *J. Allergy Clin. Immunol.* **135**, 1228-1239.

Valenzuela-Fernandez, A., Cabrero, J. R., Serrador, J. M. and Sánchez-Madrid, F. (2008). HDAC6: a key regulator of cytoskeleton, cell migration and cell–cell interactions. *Trends Cell Biol.* **18**, 291-297.

Williams, M. A. and Bevan, M. J. (2007). Effector and memory CTL differentiation. *Annu. Rev. Immunol.* **25**, 171-192.

Zhang, X., Yuan, Z., Zhang, Y., Yong, S., Salas-Burgos, A., Koomen, J., Olashaw, N., Parsons, J. T., Yang, X.-J., Dent, S. R. et al. (2007). HDAC6 modulates cell motility by altering the acetylation level of cortactin. *Mol. Cell* **27**, 197-213.